



## Structure-sensitive marker bands of metallocorroles: A resonance Raman study of manganese and gold corrole derivatives<sup>☆</sup>

James Terner <sup>a,1</sup>, Kolle E. Thomas <sup>b</sup>, Hugo Vazquez-Lima <sup>b,c</sup>, Abhik Ghosh <sup>b,\*</sup>

<sup>a</sup> Department of Chemistry, Virginia Commonwealth University, 1001 West Main Street, Richmond, VA 23284, United States of America

<sup>b</sup> Department of Chemistry and Center for Theoretical and Computational Chemistry, University of Tromsø, N-9037 Tromsø, Norway

<sup>c</sup> Centro de Química del ICUAP, Benemérita Universidad Autónoma de Puebla, 18 sur y av. San Claudio, Col. Jardines de San Manuel, C. P. 72570, Puebla, Pue, Mexico



### ABSTRACT

Soret-excited resonance Raman spectra ( $\lambda_{\text{ex}} 413.1 \text{ nm}$ ) were acquired for manganese(III) and gold(III) tris(pentafluorophenyl)corrole, each as four different isotopomeric samples: natural abundance, fully pyrrole-<sup>15</sup>N-substituted, fully meso-<sup>13</sup>C-substituted, and fully pyrrole-<sup>15</sup>N-meso-<sup>13</sup>C-substituted. The spectra were modeled with density functional theory-based vibrational analyses, which in general did an excellent job of reproducing both the absolute frequencies and isotope shifts. The results led to the assignment and visualization of approximately 10 prominent Raman bands. A key finding was that the bands could be categorized into two broad classes: Class A, exhibiting large <sup>15</sup>N isotope shifts, assignable to vibrations with predominant C<sub>α</sub>-N character, and Class B, exhibiting large meso-<sup>13</sup>C isotope shifts, assignable to vibrations with predominant C<sub>α</sub>-C<sub>meso</sub> character. Preliminary evidence suggests that the class A bands may serve as core size markers, while class B bands may correlate with the innocence or otherwise of the corrole macrocycle.

### 1. Introduction

Ever since the discovery of simple, one-pot syntheses of corroles, their chemistry has grown by leaps and bounds [1,2]. Today, the coordination chemistry of corroles is comparable in breadth and depth to that of porphyrins [3–6]. The same can be said for applications of corroles in the biomedical and technological arenas – cancer imaging and therapy [7], chemical sensors [8], and catalytic small-molecule [9], to name a handful. Vibrational spectroscopy can potentially afford deep insights into many aspects of corrole-based science and technology. Unlike for porphyrins [1–15], however, detailed IR and resonance Raman (RR) spectroscopic studies of corroles remain few and far between [16–20]. In 2015, we began a collaborative RR study of isotopically labeled manganese(III) and gold(III) corroles with the late James Terner (Jim) with a view to identifying structure-sensitive marker bands. The choice of Mn [21–23] and Au [24–33] corroles was dictated by the fact that both are paradigmatic, four-coordinate, innocent M(III) complexes, which should aid in the identification of core size marker bands. With Jim's death in March 2018, the project was sadly interrupted. The RR data he left behind has now been modeled and partially assigned with density functional theory (DFT) calculations. The results

provide one of the first, systematic studies of the skeletal vibrations of metallocorroles, including the question of structure-sensitive marker bands.

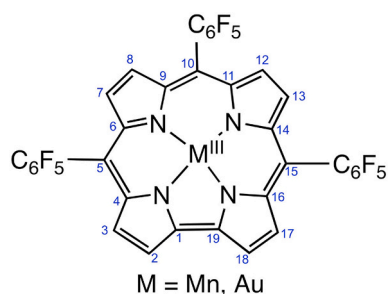
One of us (AG) first met Jim at the first International Conference on Porphyrins and Phthalocyanines (ICPP) in Dijon, France, in 2000. An authority on heme proteins, Jim was singularly respected as one who had correctly established the symmetry states and vibrational signatures of the high-valent Compound I [34,35] and Compound II [36–39] intermediates of heme proteins and model compounds (the definitive work on Compound II intermediates of heme-thiolate proteins came later from the work of Green et al. [40]). At AG's invitation, he wrote a series of critical reviews on the subject in the *Journal of Porphyrins and Phthalocyanines* [41,42], the *Journal of Biological Inorganic Chemistry* [43,44], and the *Journal of Inorganic Biochemistry* [34,45]. He also brought to bear his formidable skills as a Raman spectroscopist to another subtle problem – spin-admixed ferrihemes [46] – as well as to improved measurement of the oxygen saturation of blood [47–49]. Over the years, we enjoyed a deep friendship and many stimulating discussions at ICPP and other conferences (where we were often accompanied by our sons). In 2014, we formally collaborated for the first time, when Terner helped clarify the vibrational signatures of osmium-nitrido

<sup>☆</sup> All samples were synthesized by KET and all RR measurements were carried out by JT. All DFT calculations were carried out by HVZ. AG planned the project and composed the paper.

\* Corresponding author.

E-mail address: [abhik.ghosh@uit.no](mailto:abhik.ghosh@uit.no) (A. Ghosh).

<sup>1</sup> (Deceased March 5, 2018).



**Scheme 1.** Metallocorroles studied in this work, along with skeletal atom numbering.

corroles [50], in an early contribution to the now-vibrant field of 5d metallocorroles [4–6]. Unfortunately, we were destined to collaborate only once more, resulting in the findings described below.

## 2. Results and discussion

Two metallocorroles – Mn[TPFPC] and Au[TPFPC] [Scheme 1; TPFPC = *meso*-tris(pentafluorophenyl)corrole] – were each studied in 4

different isotopomeric forms: natural abundance, fully pyrrole-<sup>15</sup>N-substituted, fully *meso*-<sup>13</sup>C-substituted, and fully pyrrole-<sup>15</sup>N-*meso*-<sup>13</sup>C-substituted. Both molecules were optimized under a *C*<sub>2</sub> symmetry constraint, which resulted in no imaginary frequencies. Fig. 1 depicts the Soret-excited ( $\lambda_{\text{ex}} = 413.1$  nm) RR spectra of all eight species over 250–2000 cm<sup>-1</sup>. Table 1 lists the frequencies of potential structure-sensitive RR bands and potential scalar-relativistic DFT (ZORA-BP86-D3/ZORA-STO-TZ2P) counterparts. Table 2 recasts the data in the form of isotope shifts and identifies calculated vibrations whose isotope shifts best match the experimental values. Fig. 2 depicts selected optimized geometries of the two molecules; only marginal differences were observed for the C<sub>α</sub>-C<sub>β</sub> and C<sub>β</sub>-C<sub>β</sub> bonds between the two molecules. Figs. 3–8 present visual depictions of selected, calculated eigenvectors. The results underscore the following points.

The main conclusion arising out of the data is that majority of the prominent vibrations in the Raman spectra may be categorized into two broad classes: class A, with larger <sup>15</sup>N isotope shifts but small *meso*-<sup>13</sup>C isotope shifts, and class B, with larger *meso*-<sup>13</sup>C isotope shifts but smaller <sup>15</sup>N isotope shifts. The calculated results provide broad support for this finding: class A vibrations involve predominantly C<sub>α</sub>-N stretching, whereas class B vibrations involve predominantly C<sub>α</sub>-C<sub>meso</sub> stretching. Given the low symmetry of the corrole macrocycle, several vibrations, understandably, involve both C<sub>α</sub>-N and C<sub>α</sub>-C<sub>meso</sub> character, but one

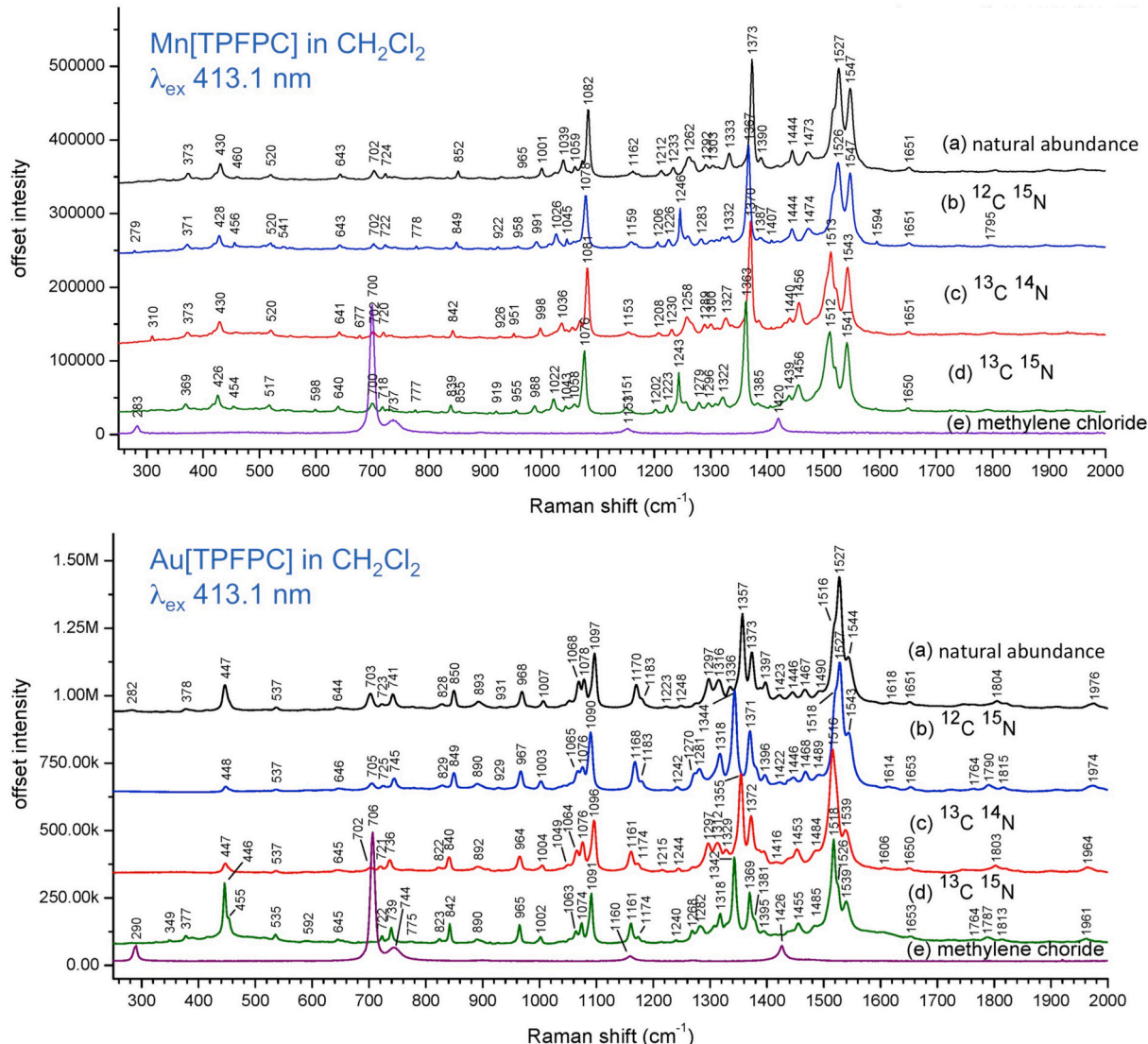


**Fig. 1.** Resonance Raman spectra ( $\lambda_{\text{ex}} = 413.1$  nm) of Mn[TPFPC] and Au[TPFPC] in dichloromethane.

**Table 1**Selected RR frequencies ( $\nu_{RR}$ ,  $\text{cm}^{-1}$ ) in  $\text{CH}_2\text{Cl}_2$  and potential DFT counterparts ( $\nu_{DFT}$ ,  $\text{cm}^{-1}$ ) for different isotopomers.

Metal	$\nu_{RR}$				$\nu_{DFT}$				$\nu_{RR}/\nu_{DFT}$			
	$^{12}\text{C}^{14}\text{N}$	$^{13}\text{C}^{14}\text{N}$	$^{12}\text{C}^{15}\text{N}$	$^{13}\text{C}^{15}\text{N}$	$^{12}\text{C}^{14}\text{N}$	$^{13}\text{C}^{14}\text{N}$	$^{12}\text{C}^{15}\text{N}$	$^{13}\text{C}^{15}\text{N}$	$^{12}\text{C}^{14}\text{N}$	$^{13}\text{C}^{14}\text{N}$	$^{12}\text{C}^{15}\text{N}$	$^{13}\text{C}^{15}\text{N}$
Au	447	447	448	446	440.0	439.7	438.1	437.8	1.0158	1.0166	1.0226	1.0188
Mn	430	430	428	426	415.9	416.0	415.0	415.1	1.0339	1.0337	1.0313	1.0263
Au	537	537	537	535	531.5	530.8	528.2	527.7	1.0104	1.0116	1.0166	1.0139
Mn	520	520	520	517	518.2	517.8	515.7	515.3	1.0035	1.0042	1.0083	1.0033
Au	850	840	849	842	845.5	836.8	843.1	834.7	1.0054	1.0038	1.0070	1.0087
					848.1	838.9	844.7	835.7	1.0023	1.0013	1.0051	1.0075
Mn	852	842	849	839	847.8	840.3	845.0	837.9	1.0050	1.0020	1.0047	1.0013
					849.7	841.7	846.1	838.3	1.0027	1.0004	1.0034	1.0008
Au	1007	1004	1003	1002	1001.4	999.8	995.1	993.4	1.0056	1.0042	1.0080	1.0086
Mn	1001	998	991	988	996.5	994.8	987.5	985.9	1.0045	1.0032	1.0035	1.0021
Au	1097	1096	1090	1091	1092.0	1091.9	1083.9	1083.8	1.0046	1.0037	1.0056	1.0066
Mn	1082	1081	1078	1076	1081.3	1081.1	1076.7	1076.4	1.0006	0.9999	1.0012	0.9996
Au	1170	1161	1168	1161	1168.4	1160.3	1165.1	1156.3	1.0013	1.0006	1.0025	1.0040
Mn	1162	1153	1159	1151	1157.7	1149.8	1153.2	1145.5	1.0037	1.0028	1.0051	1.0048
Au	1297	1297	1281	1282	1282.9	1282.1	1267.1	1267.0	1.0110	1.0116	1.0110	1.0118
					1286.7	1284.3	1284.3	1282.6	1.0080	1.0099	0.9974	0.9995
					1294.9	1293.4	1283.6	1282.7	1.0016	1.0028	0.9980	0.9995
Mn	1292	1289	1283	1279	1238.1	1237.5	1226.9	1226.2	1.0193	1.0166	1.0156	1.0137
					1281.6	1280.6	1279.4	1278.6	0.9847	0.9824	0.9739	0.9722
					1258.4	1257.6	1248.9	1248.4	1.0029	1.0003	0.9977	0.9957
Au	1357	1355	1343	1342	1362.2	1361.3	1355.3	1353.5	0.9962	0.9953	0.9909	0.9915
					1377.3	1374.6	1368.9	1365.5	0.9853	0.9858	0.9810	0.9828
Mn	1373	1370	1367	1363	1361.1	1357.1	1355.0	1350.1	1.0087	1.0095	1.0089	1.0096
					1373.3	1368.4	1371.6	1366.6	0.9998	1.0012	0.9966	0.9974
Au	1467	1453	1468	1455	1471.5	1463.8	1470.3	1462.9	0.9969	0.9926	0.9984	0.9946
Mn	1473	1456	1474	1456	1478.0	1469.0	1477.6	1468.4	0.9966	0.9912	0.9976	0.9916
					1481.7	1476.0	1481.6	1475.6	0.9941	0.9864	0.9949	0.9867
Au	1527	1516	1527	1518	1503.6	1487.8	1501.7	1486.8	1.0155	1.0189	1.0168	1.0210
					1508.5	1499.9	1507.0	1497.1	1.0123	1.0107	1.0133	1.0140
Mn	1527	1513	1526	1512	1505.9	1500.9	1505.1	1500.1	1.0140	1.0081	1.0139	1.0079
					1518.8	1496.0	1518.4	1495.4	1.0054	1.0114	1.0050	1.0111
Au	1544	1539	1543	1539	1515.9	1511.2	1514.8	1510.0	1.0185	1.0184	1.0186	1.0192
					1531.9	1528.7	1531.0	1527.9	1.0079	1.0067	1.0078	1.0072
Mn	1547	1543	1547	1541	1518.9	1512.6	1518.3	1512.0	1.0185	1.0201	1.0189	1.0192
					1555.2	1553.5	1555.1	1553.4	0.9947	0.9932	0.9948	0.9920

**Table 2**Experimentally observed  $^{15}\text{N}$  and *meso*- $^{13}\text{C}$  isotope shifts of key structure-sensitive bands and the most plausible DFT assignments.

Metal	$\nu_{\text{unlabelled}}$ ( $\text{cm}^{-1}$ )	$\Delta\nu_{15\text{N}}$ ( $\text{cm}^{-1}$ )	$\nu_{\text{meso-13C}}$ ( $\text{cm}^{-1}$ )	$\Delta\nu_{13\text{C}}$ ( $\text{cm}^{-1}$ )	$\Delta\nu_{15\text{N}}$ ( $\text{cm}^{-1}$ ) <sup>a</sup>	$\nu_{\text{DFT}}$ ( $\text{cm}^{-1}$ )
Group A: Vibrational modes with substantial/predominant $\text{C}_{\alpha}\text{-N}$ character						
Mn	1373	-6	1370	-3	-7	1361.1
Au	1357	-14	1355	-2	-13	1362.2
Mn	1292	-9	1289	-3	-15	1281.6
Au	1297	-16	1297	-0	-15	1286.7
Mn	1082	-4	1081	-1	-5	1082.7
Au	1097	-7	1096	-1	-5	1092.0
Mn	1001	-10	998	-3	-10	996.5
Au	1007	-4	1004	-3	-2	1001.4
Group B: Vibrational modes with substantial/predominant $\text{C}_{\alpha}\text{-C}_{\text{meso}}$ character						
Mn	1547	0	1543	-4	-1	1555.2
Au	1544	-1	1539	-5	0	1531.9
Mn	1527	-1	1513	-14	-1	1518.9
Au	1527	0	1516	-11	0	1515.9
Mn	1473	1	1456	-17	-3	1481.7
Au	1467	1	1453	-14	-2	1472.6
Mn	1162	-3	1153	-9	-2	1157.7
Au	1170	-2	1161	-9	0	1168.4
Mn	852	-3	842	-10	-3	847.8
Au	850	-1	840	-10	-2	845.5

usually predominates. Importantly, these two classes do not refer to the irreducible representations of the  $C_2$  point group. The great majority of the observed Raman-active vibrations appear to belong to the A irrep; however, certain vibrations belonging to the B irrep are potentially also Raman-active.

**Table 2** identifies four vibrations with predominant or substantial  $\text{C}_{\alpha}\text{-N}$  character, all in the 950–1400  $\text{cm}^{-1}$  range. Of these, only the vibration around 1360  $\text{cm}^{-1}$  can be described as a breathing mode; the other three vibrations preferentially involve only one of the two symmetry-distinct pairs of central nitrogens. For all four vibrations,  $\nu_{\text{DFT}}$  is slightly higher for Au than for Mn, suggesting stronger metal-nitrogen bonds with higher stretching force-constants for Au (even though kinematic considerations might have suggested the reverse). However, the complex interplay of kinematic and dynamic factors in these complexes makes such an interpretation uncertain. Be that as it may, these four vibrations appear most suited as core size markers.

Of the five vibrations identified as having predominant or substantial  $\text{C}_{\alpha}\text{-C}_{\text{meso}}$  character, the highest-frequency vibration, with  $\nu_{\text{DFT}}$  (Mn, Au) = 1555.2, 1531.9  $\text{cm}^{-1}$ , also has substantial C1-C19 (direct pyrrole-pyrrole linkage) character. Preliminary evidence from an earlier IR and DFT studies of Fe corroles suggest that the vibrations may serve as markers for a noninnocent macrocycle in metallocorroles (which exhibit characteristic bond length alternations for the corrole skeleton). However, vibrational analyses of a wider range of compounds, and appropriate isotopomers, are warranted before such studies can be considered

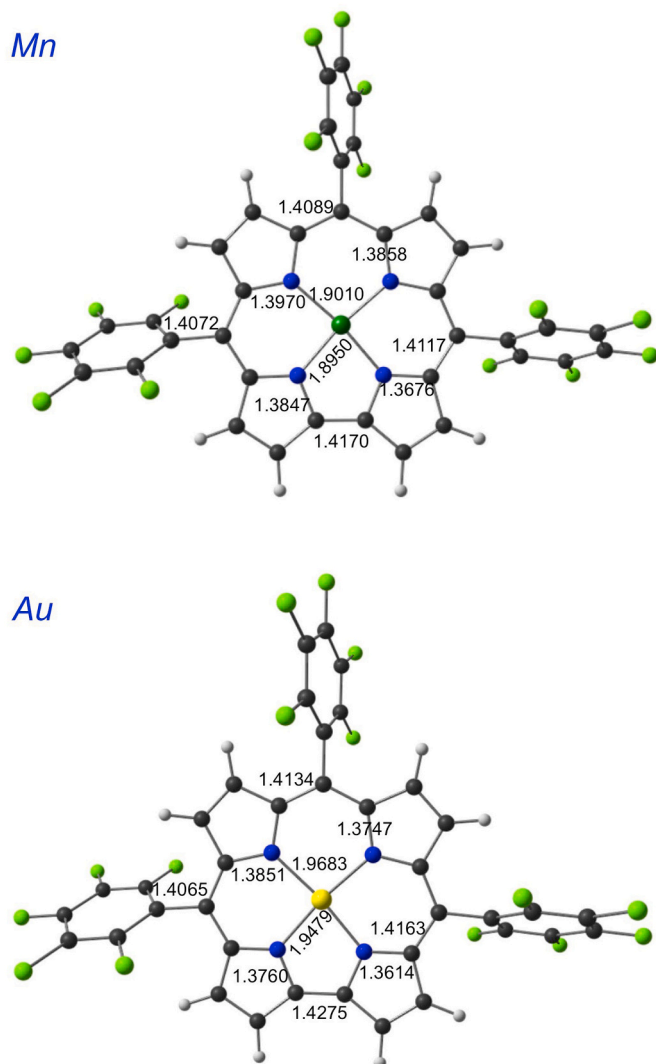


**Fig. 2.** Selected distances ( $\text{\AA}$ ) in the optimized geometries of Mn[TPFPC] and Au[TPFPC]. Note that the Au—N distances are 0.05  $\text{\AA}$  or more longer than the corresponding Mn—N distances.

widely useful.

### 3. Conclusion

A combined resonance Raman and DFT study of planar Mn(III) and Au(III) corroles has led to the assignment of approximately ten prominent bands, filling a significant knowledge gap relative to the physicochemical properties of metallocorroles. Based on  $^{15}\text{N}$  and *meso*- $^{13}\text{C}$  isotope shifts, the bands fall into two major classes: class A, with predominant or substantial  $\text{C}_{\alpha}\text{N}$  character, and class B, with predominant or substantial  $\text{C}_{\alpha}\text{C}_{\text{meso}}$  character. The former appear more relevant as core size marker bands, while the latter may shed light on the innocence or noninnocence of the corrole macrocycle. That said, the increased mixing of internal coordinates in corrole normal modes (relative to porphyrins) may ultimately limit their use as geometric and electronic markers.

## 4. Experimental section

### 4.1. Synthetic methods

*N,N*-dimethylformamide (carbonyl- $^{13}\text{C}$ , 99%) and pyrrole- $^{15}\text{N}$  (98%) were purchased from Cambridge Isotopes Laboratories, Inc., and used as received. Silica (150  $\text{\AA}$  pore size, 35–70  $\mu\text{m}$  particle size, Davisil) was used for flash chromatography and silica gel 60 preparative thin-layer chromatographic (PTLC) plates (20 × 20 cm; 0.5 mm thick, Merck) for further purification. Pentafluorobenzaldehyde- $^{13}\text{CHO}$  was prepared as previously reported [51], as were free-base tris(pentafluorophenyl) corrole,  $\text{H}_3[\text{TPFPC}]$  [52,53], and its *meso*- $^{13}\text{C}$ , pyrrole- $^{15}\text{N}$ , and *meso*- $^{13}\text{C}$ -pyrrole- $^{15}\text{N}$  -labeled analogues. Natural-abundance and labeled Mn[TPFPC] [22] and Au[TPFPC] [26,31] were also prepared as previously reported, with minor modifications for the Au complex.

Gold acetate (5 eq, 141 mg, 0.37 mmol) was added to a pyridine (10 mL) solution of  $\text{H}_3[\text{TPFPC}]$  (60 mg, 0.075 mmol). The reaction mixture was stirred overnight, followed by evaporation of the solvent. The residue was chromatographed on a silica gel column with 4:1 n-hexane/ $\text{CH}_2\text{Cl}_2$ , yielding Au[TPFPC] as the first red band. PTLC with 3:1 hexane/ $\text{CH}_2\text{Cl}_2$  yielded the pure complex as the first scarlet band (3.8 mg, 5.2%), with spectroscopic data matching those reported earlier [31].

Electrospray ionization (ESI) mass spectra were recorded in the positive mode on an LTQ Orbitrap XL spectrometer for all isotopomeric complexes. Infrared spectra were obtained on dry, solid samples via attenuated total reflection on a Varian 700e FT-IR spectrometer.

### 4.2. Resonance Raman measurements

Resonance Raman spectra were obtained as previously reported [50], using a Coherent Sabre DBW krypton ion laser, generally with an excitation wavelength of 413.1 nm. Samples were prepared by placing microgram quantities of the solid compounds inside melting point capillaries, and adding dichloromethane to obtain an optical density of approximately 1.0 at the wavelength of the laser. A laser power of ~0.7 mW was focused to a 100  $\mu\text{m}$  diameter spot at the sample. Raman signal was collected at 90 degrees with a Canon f/0.95 50 mm camera lens and focused onto a 75  $\mu\text{m}$  slit aperture of a 0.5 m Spex (Horiba) model 1870 spectrograph containing a single Jobin Yvon (Horiba) 1200 lines/mm holographic grating. Kaiser Optical holographic filters were used to filter the laser scattered light when necessary. Mounted on the spectrograph was a liquid nitrogen cooled Pylon CCD detector from Princeton Instruments. Indene and toluene were used for wavelength calibration.

### 4.3. DFT calculations

The structures were optimized in gas phase with the scalar ZORA [54,55] Hamiltonian, the BP86 [56,57] exchange-correlation functional, Grimme's D3 [58,59] dispersion corrections and all-electron Slater-type TZ2P basis sets, all as implemented in the ADF program system [60]. The tightest practicable criteria were used for both SCF and geometry cycles as well as for frequency analyses; the latter established the optimized structures as true minima.

### Author statement

James Terner: Resonance Raman spectroscopy. Kolle E. Thomas: Synthesis and compound characterization. Hugo Vazquez-Lima: DFT calculations and interpretation. Abhik Ghosh: Overall planning, supervision, funding, and writing of the paper.

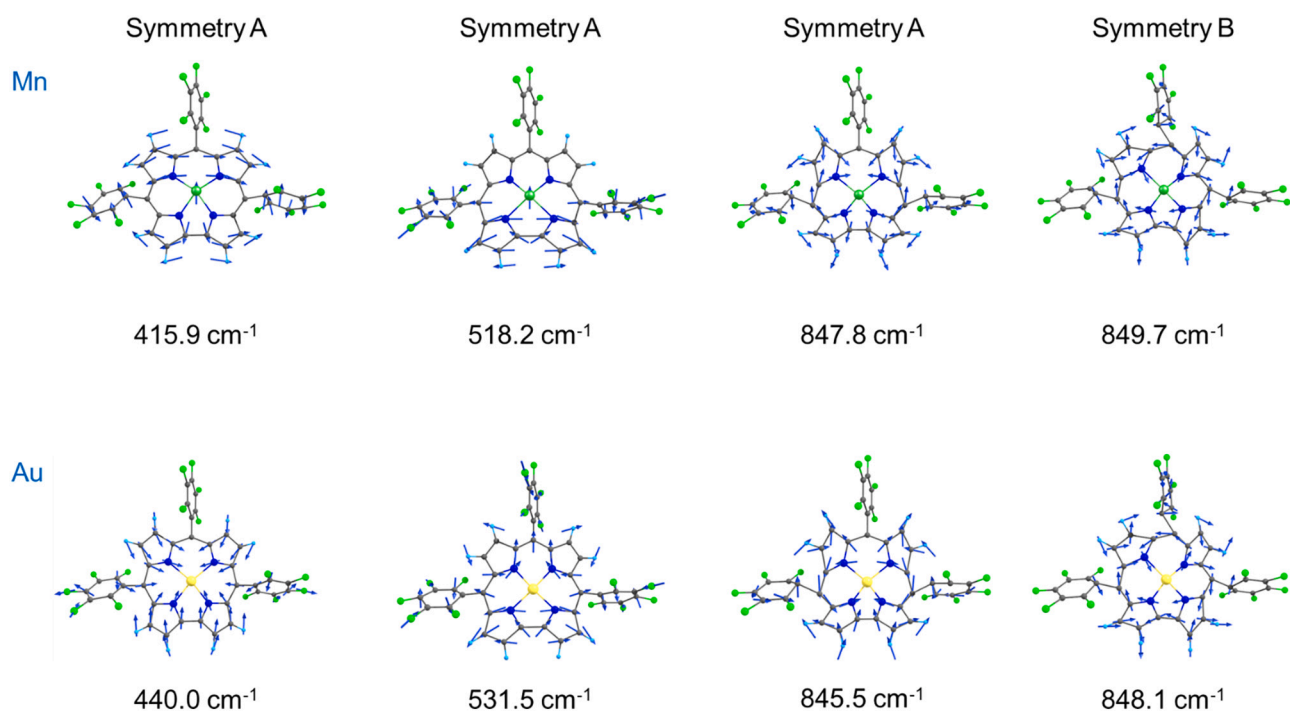


**Fig. 3.** Eigenvectors and corresponding DFT frequencies for potential structure-sensitive RR bands below 900 cm<sup>-1</sup>. The frequencies refer to the <sup>12</sup>C<sup>14</sup>N column under  $\nu_{\text{DFT}}$  in Table 1.

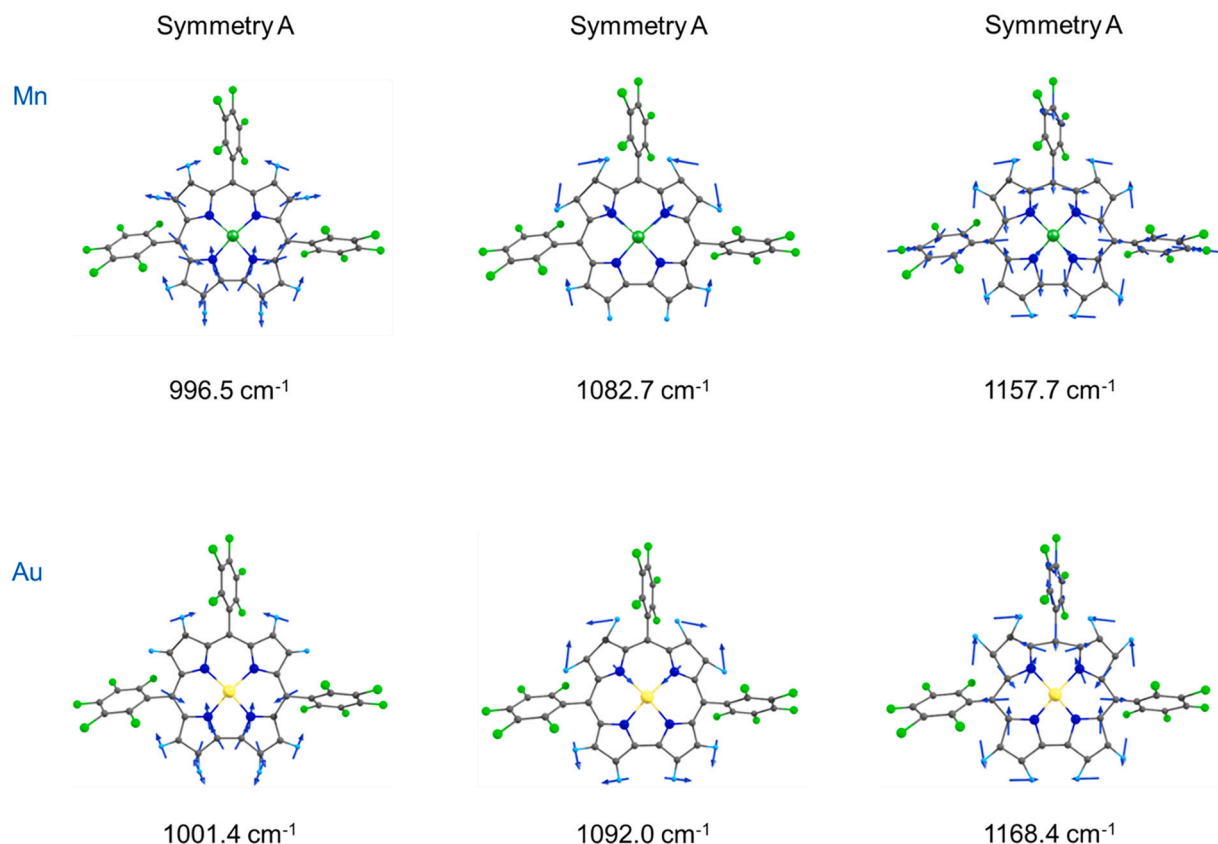


**Fig. 4.** Eigenvectors and corresponding DFT frequencies for potential structure-sensitive RR bands in the 900–1200 cm<sup>-1</sup> region. The frequencies refer to the <sup>12</sup>C<sup>14</sup>N column under  $\nu_{\text{DFT}}$  in Table 1.

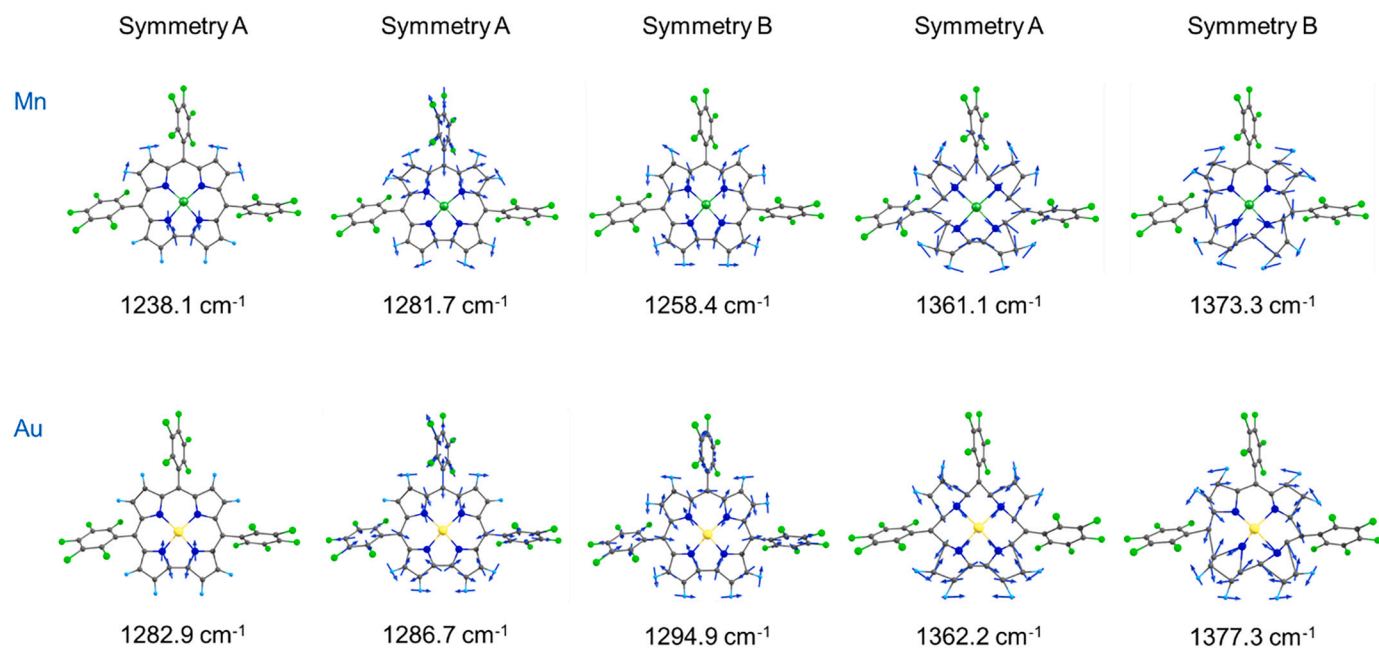


**Fig. 5.** Eigenvectors and corresponding DFT frequencies for potential structure-sensitive RR bands in the 1200–1400  $\text{cm}^{-1}$  region. The frequencies refer to the  $^{12}\text{C}^{14}\text{N}$  column under  $\nu_{\text{DFT}}$  in Table 1.

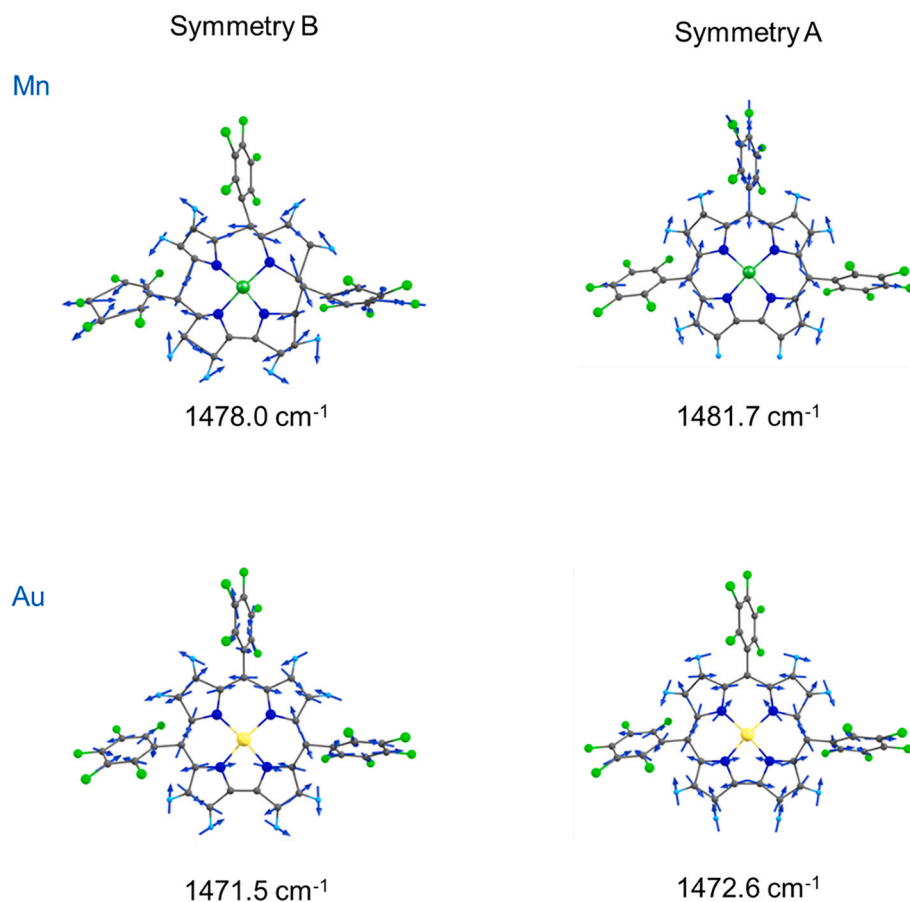


**Fig. 6.** Eigenvectors and corresponding DFT frequencies for potential structure-sensitive RR bands in the 1400–1500  $\text{cm}^{-1}$  region. The frequencies refer to the  $^{12}\text{C}^{14}\text{N}$  column under  $\nu_{\text{DFT}}$  in Table 1.

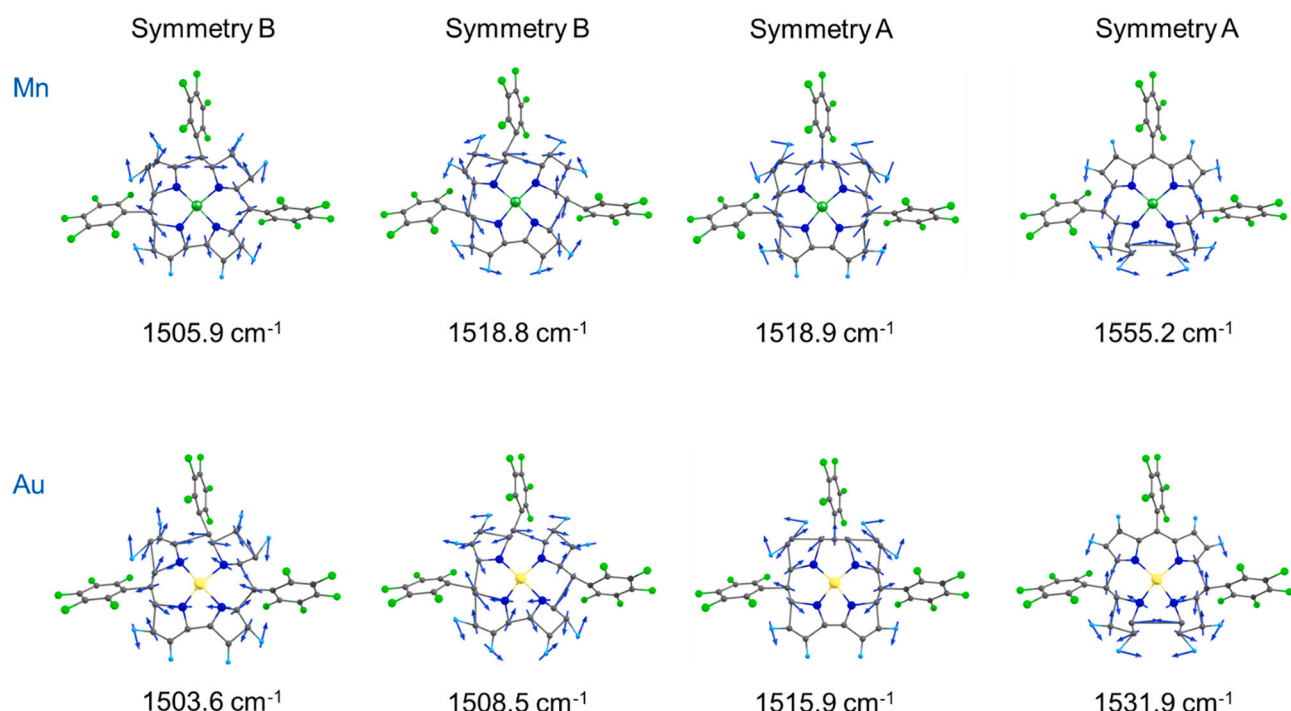


**Fig. 7.** Eigenvectors and corresponding DFT frequencies for potential structure-sensitive RR bands in the 1500–1500 cm<sup>-1</sup> region. The frequencies refer to the <sup>12</sup>C<sup>14</sup>N column under  $\nu_{\text{DFT}}$  in Table 1.

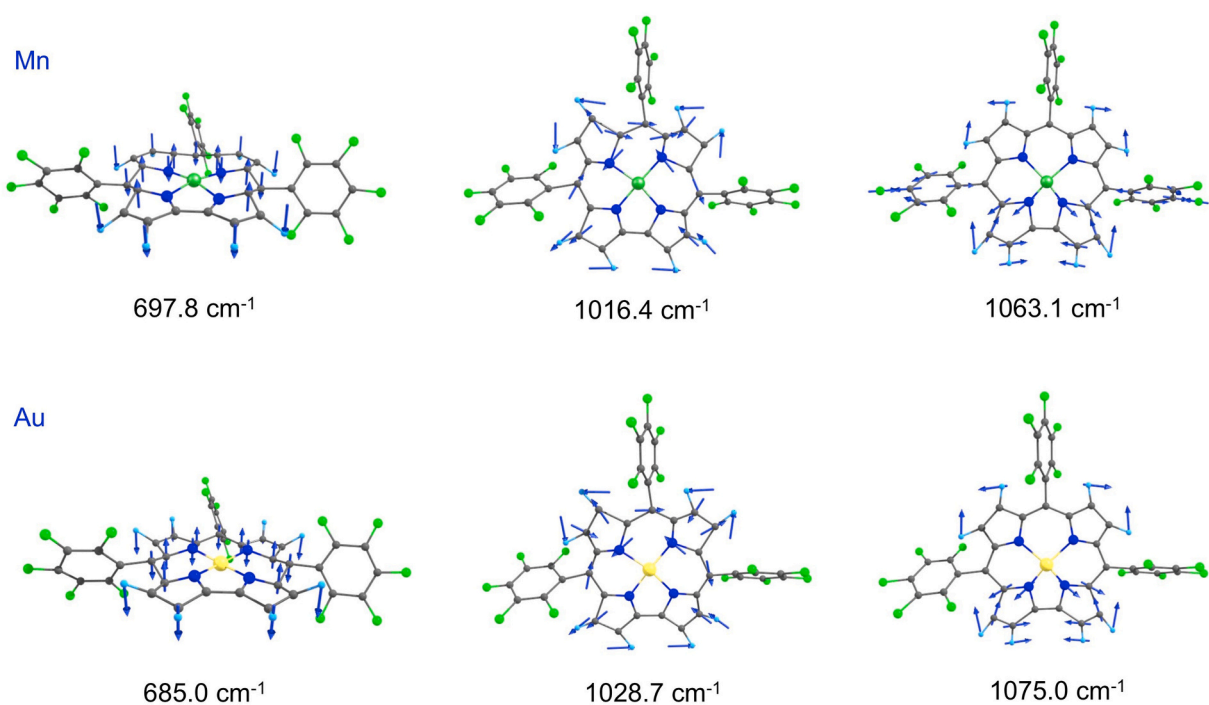


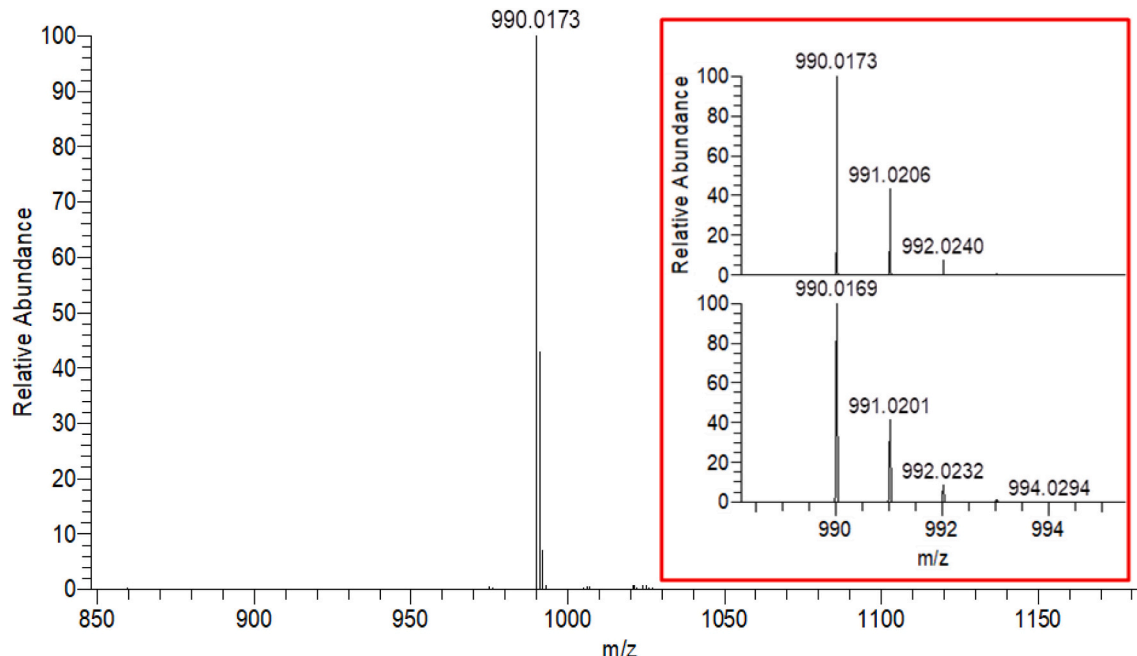
**Fig. 8.** Eigenvectors and corresponding DFT frequencies for potential structure-sensitive IR bands. The frequencies refer to the <sup>12</sup>C<sup>14</sup>N column under  $\nu_{\text{DFT}}$  in Table 2.

**Declaration of Competing Interest**

None.

**Acknowledgement**

This work was supported in part by grant nos. 262229 and 324139 from the Research Council of Norway.

**Appendix A. ESI mass spectra**

**Fig. A1.** Positive-mode ESI mass spectrum of natural-abundance Au[TPFPC]. Insert: Detail of the molecular ion peak (top) and simulation (bottom). Molecular formula:  $\text{N}_4\text{F}_{15}\text{C}_{37}\text{H}_8\text{Au}$ .

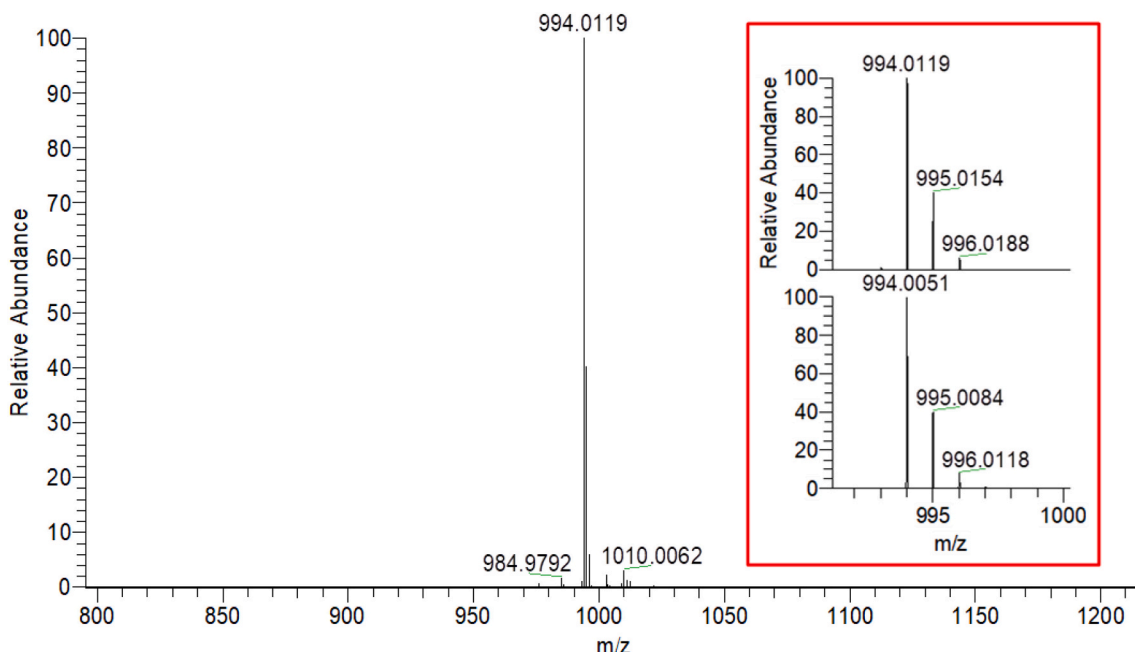


**Fig. A2.** Positive-mode ESI mass spectrum of fully pyrrole- $^{15}\text{N}$ -substituted Au[TPFPC]. Insert: Detail of the molecular ion peak (top) and simulation (bottom). Molecular formula:  $^{15}\text{N}_4\text{F}_{15}\text{C}_{37}\text{H}_8\text{Au}$ .

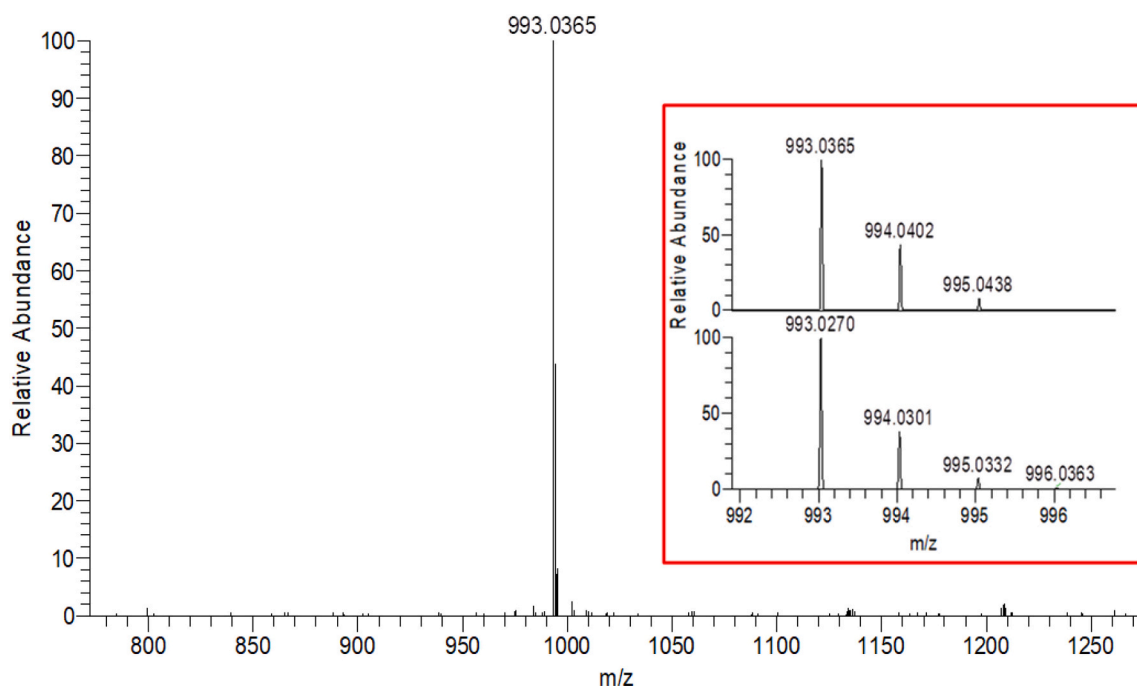


**Fig. A3.** Positive-mode ESI mass spectrum of fully *meso*-<sup>13</sup>C-substituted Au[TPFPC]. Insert: Detail of the molecular ion peak (top) and simulation (bottom). Molecular formula: <sup>13</sup>C<sub>3</sub>N<sub>4</sub>F<sub>15</sub>C<sub>34</sub>H<sub>8</sub>Au.

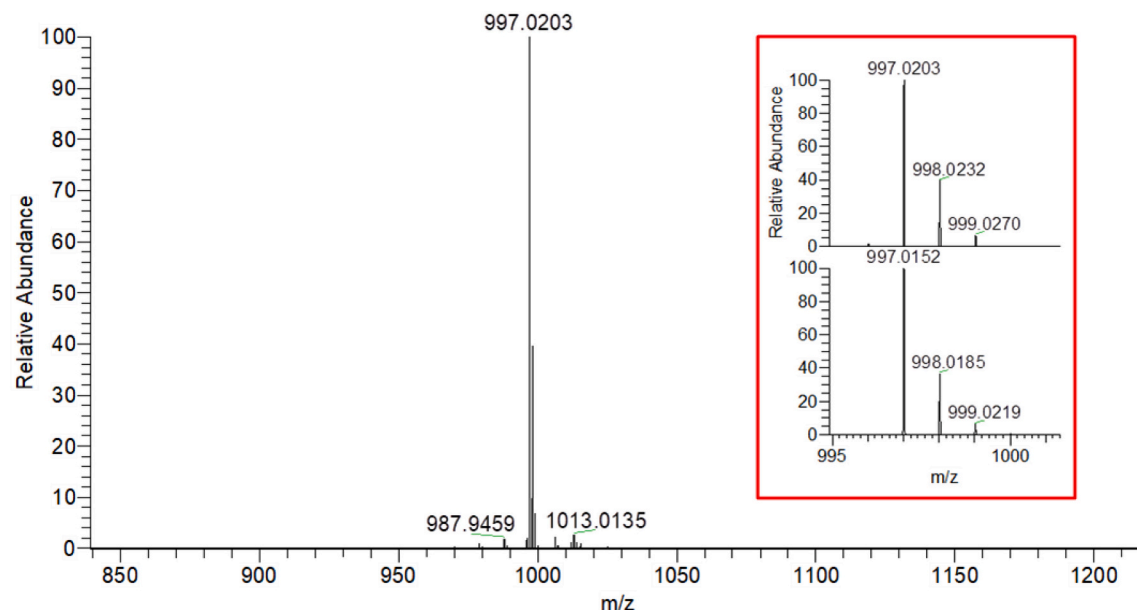


**Fig. A4.** Positive-mode ESI mass spectrum of fully *meso*-<sup>13</sup>C- and pyrrole-<sup>15</sup>N-substituted Au[TPFPC]. Insert: Detail of the molecular ion peak (top) and simulation (bottom). Molecular formula: <sup>13</sup>C<sub>3</sub><sup>15</sup>N<sub>4</sub>F<sub>15</sub>C<sub>34</sub>H<sub>8</sub>Au.

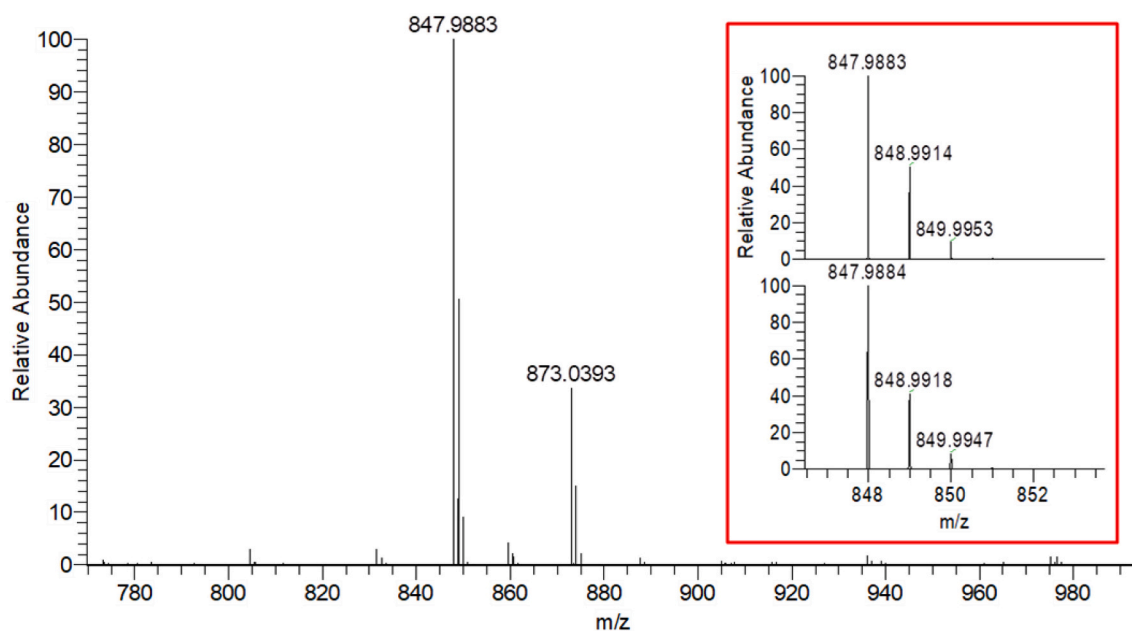


**Fig. A5.** Positive-mode ESI mass spectrum of natural-abundance Mn[TPFPC]. Insert: Detail of the molecular ion peak (top) and simulation (bottom). Molecular formula:  $\text{N}_4\text{F}_{15}\text{C}_{37}\text{H}_8\text{Mn}$ .

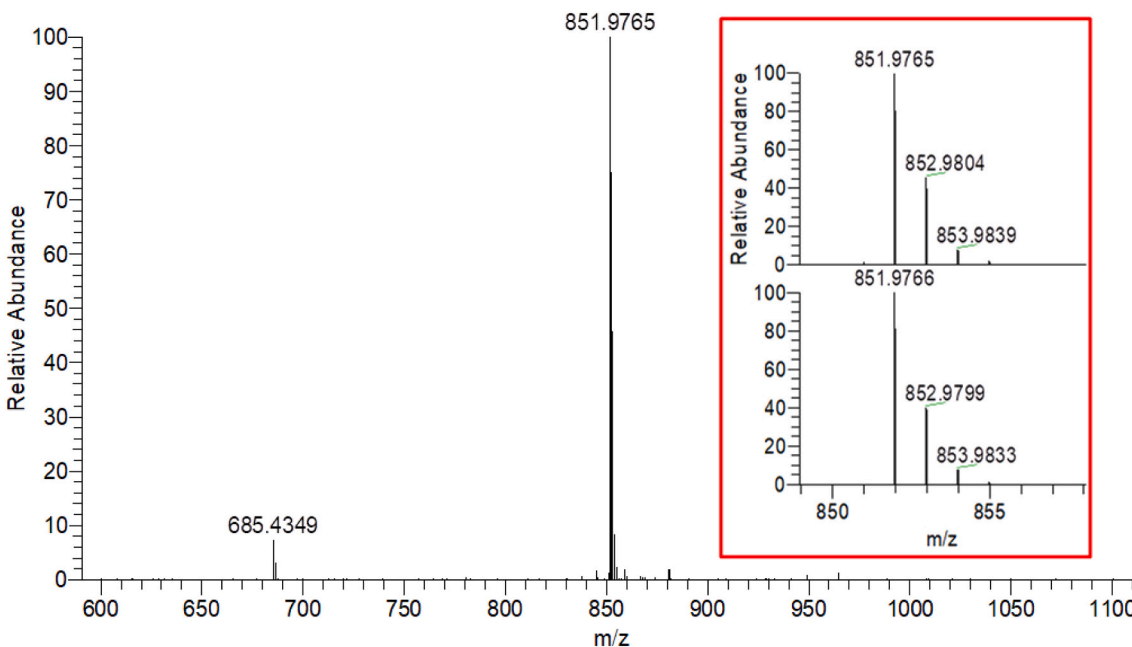


**Fig. A6.** Positive-mode ESI mass spectrum of fully pyrrole- $^{15}\text{N}$ -substituted Mn[TPFPC]. Insert: Detail of the molecular ion peak (top) and simulation (bottom). Molecular formula:  $^{15}\text{N}_4\text{F}_{15}\text{C}_{37}\text{H}_8\text{Mn}$ .

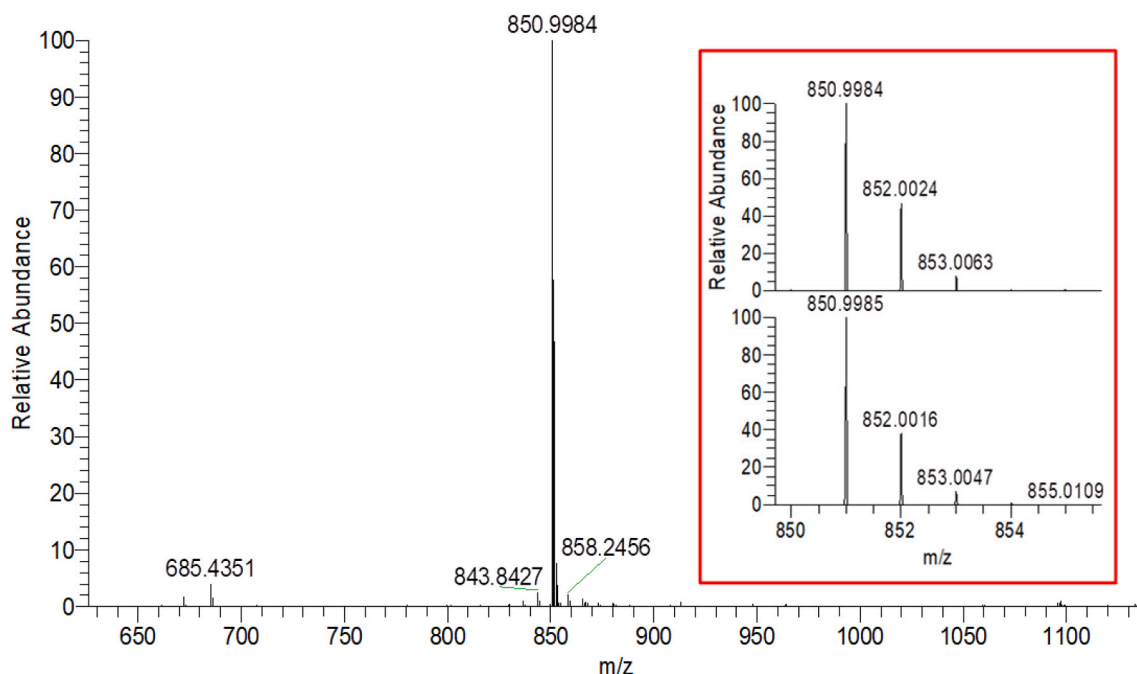


**Fig. A7.** Positive-mode ESI mass spectrum of fully *meso*-<sup>13</sup>C-substituted Mn[TPFPC]. Insert: Detail of the molecular ion peak (top) and simulation (bottom). Molecular formula: <sup>13</sup>C<sub>3</sub>N<sub>4</sub>F<sub>15</sub>C<sub>34</sub>H<sub>8</sub>Mn.

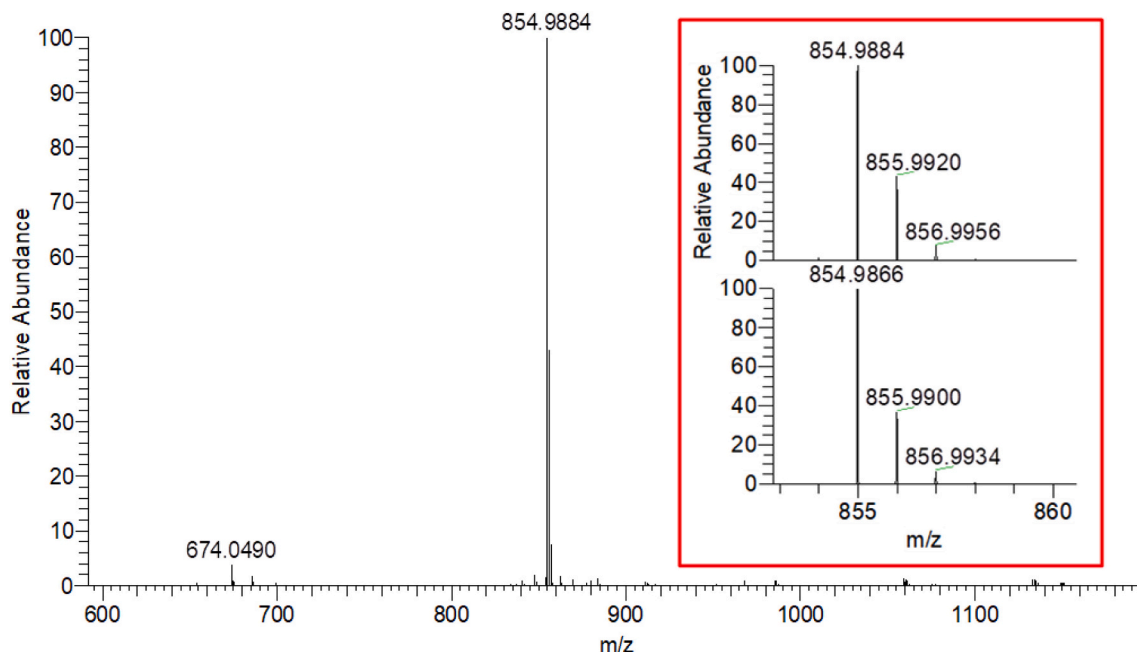


**Fig. A8.** Positive-mode ESI mass spectrum of fully *meso*-<sup>13</sup>C- and pyrrole-<sup>15</sup>N-substituted Mn[TPFPC]. Insert: Detail of the molecular ion peak (top) and simulation (bottom). Molecular formula: <sup>13</sup>C<sub>3</sub><sup>15</sup>N<sub>4</sub>F<sub>15</sub>C<sub>34</sub>H<sub>8</sub>Mn.

## References

- [1] R. Orlowski, D. Gryko, D.T. Gryko, Synthesis of Corroles and their Heteroanalogs, Chem. Rev. 117 (2017) 3102–3137.
- [2] J.F.B. Barata, M.G.P.M.S. Neves, M.A.F. Fautino, A.C. Tomé, J.A.S. Cavaleiro, Strategies for Corrole Functionalization, Chem. Rev. 117 (2017) 3192–3253.
- [3] K.E. Thomas, A.B. Alemayehu, J. Conradi, C.M. Beavers, A. Ghosh, The structural chemistry of metallocorroles: combined X-ray crystallography and quantum chemistry studies afford unique insights, Acc. Chem. Res. 45 (2012) 1203–1214.
- [4] A. Ghosh, Electronic structure of corrole derivatives: insights from molecular structures, spectroscopy, electrochemistry, and quantum chemical calculations, Chem. Rev. 117 (2017) 3798–3881.
- [5] S. Nardis, F. Mandoj, M. Stefanelli, R. Paolesse, Metal complexes of corrole, Coord. Chem. Rev. 388 (2019) 360–405.
- [6] A.B. Alemayehu, K.E. Thomas, R.F. Einrem, A. Ghosh, Acc. Chem. Res. 54 (2021) 3095–3107.
- [7] R.D. Teo, J.Y. Hwang, J. Termini, Z. Gross, H.B. Gray, Fighting cancer with corroles, Chem. Rev. 117 (2017) 2711–2729.
- [8] R. Paolesse, S. Nardis, D. Monti, M. Stefanelli, C. Di Natale, Porphyrinoids for chemical sensor applications, Chem. Rev. 117 (2017) 2517–2583.
- [9] W. Zhang, L. Wenzhen, R. Cao, Energy-related small molecule activation reactions: oxygen reduction and hydrogen and oxygen evolution reactions catalyzed by porphyrin- and corrole-based systems, Chem. Rev. 117 (2017) 3717–3797.
- [10] T. Kitagawa, Y. Ozaki, Infrared and Raman spectra of metalloporphyrins, Struct. Bond. 64 (1987) 71–114, <https://doi.org/10.1007/BFb0036790>.
- [11] L.D. Spaulding, C.C. Chang, N.T. Yu, R.H. Felton, Resonance Raman spectra of metallooctaethylporphyrins. Structural probe of metal displacement, J. Am. Chem. Soc. 97 (1975) 2517–2525.

- [12] T.G. Spiro, Resonance Raman spectroscopy as a probe of heme protein structure and dynamics, *Adv. Protein Chem.* 37 (1985) 111–159. <https://www.sciencedirect.com/science/article/abs/pii/S0065323308600649>.
- [13] S. Hu, T.G. Spiro, The origin of infrared marker bands of porphyrin  $\pi$ -cation radicals: infrared assignments for cations of copper(II) complexes of octaethylporphine and tetraphenylporphine, *J. Am. Chem. Soc.* 115 (1993) 12029–12034.
- [14] N. Parthasarathi, C. Hansen, S. Yamaguchi, T.G. Spiro, Metalloporphyrin core size resonance Raman marker bands revisited: implications for the interpretation of hemoglobin photoproduct Raman frequencies, *J. Am. Chem. Soc.* 109 (1987) 3865–3871.
- [15] I. Halvorsen, E. Steene, A. Ghosh, Resonance Raman marker bands of  $\beta$ -octahalogeno-meso-tetraarylmetalloporphyrins, *J. Porphyrins Phthalocyanines* 5 (2001) 721–730.
- [16] I.H. Wondimagegn, A. Ghosh, Electronic absorption, resonance Raman, and electrochemical studies of planar and saddled copper(III) meso-triarylcorroles. Highly substituent-sensitive Soret bands as a distinctive feature of high-valent transition metal corroles, *J. Am. Chem. Soc.* 124 (2002) 8104–8116.
- [17] E. Steene, T. Wondimagegn, A. Ghosh, Resonance Raman spectroscopy and density functional theoretical calculations of manganese corroles: a parallelism between high-valent metalloporphyrins, relevant to horseradish peroxidase and chloroperoxidase compound I and II intermediates, *J. Inorg. Biochem.* 88 (2002) 113–118.
- [18] H. Vazquez-Lima, H.K. Norheim, R.F. Einrem, A. Ghosh, Cryptic noninnocence: FeNO Corroles in a new light, *Dalton Trans.* 44 (2015) 10146–10151.
- [19] M.H. Rahman, M.D. Ryan, H. Vazquez-Lima, A. Alemanyehu, A. Ghosh, Infrared spectroelectrochemistry of iron-nitrosyl triarylcorroles, implications for ligand noninnocence, *Inorg. Chem.* 59 (2020) 3232–3238.
- [20] S. Ganguly, A. Ghosh, Seven clues to ligand noninnocence: the metalloporphyrin paradigm, *Acc. Chem. Res.* 52 (2019) 2003–2014.
- [21] H.-Y. Liu, M.H.R. Mahmood, S.-X. Qiu, C.K. Chang, Recent developments in manganese corrole chemistry, *Coord. Chem. Rev.* 257 (2013) 1306–1333.
- [22] Z. Gross, G. Golubkov, L. Simkovich, Epoxidation catalysis by a manganese corrole and isolation of an oxomanganese(V) corrole, *Angew. Chem. Int. Ed.* 39 (2000) 4045–4047.
- [23] Z. Ou, C. Erben, M. Autret, S. Will, D. Rosen, J. Lex, E. Vogel, K.M. Kadish, Manganese(III) and manganese(IV) corroles: synthesis, spectroscopic, electrochemical and X-ray structural characterization, *J. Porphyrins Phthalocyanines* 9 (2005) 398–412.
- [24] A.B. Alemanyehu, A. Ghosh, Gold Corroles, *J. Porphyrins Phthalocyanines* 15 (2011) 106–110.
- [25] E. Rabinovitch, I. Goldberg, Z. Gross, Gold(I) and Gold(III) Corroles, *Chem. Eur. J.* 17 (2011) 12294–12301.
- [26] K.E. Thomas, A.B. Alemanyehu, J. Conradie, C. Beavers, A. Ghosh, Synthesis and molecular structure of gold triarylcorroles, *Inorg. Chem.* 50 (2011) 12844–12851.
- [27] K.E. Thomas, C.M. Beavers, A. Ghosh, Molecular structure of a gold  $\beta$ -octakis (trifluoromethyl)-meso-triarylcorrole: an 85° difference in saddling dihedral relative to copper, *Mol. Phys.* 110 (2012) 2439–2444.
- [28] J. Capar, J. Zonneveld, S. Berg, J. Isaksson, K.J. Gagnon, K.E. Thomas, A. Ghosh, Demetalation of copper undecaarylcorroles: molecular structures of a free-base undecaarylcorrole and a gold undecaarylcorrole, *J. Inorg. Biochem.* 162 (2016) 146–153.
- [29] K.E. Thomas, K.J. Gagnon, L.J. McCormick, A. Ghosh, Molecular structure of gold 2,3,7,8,12,13,17,18-octabromo-5,10,15-tris(4"-pentafluorosulfanylphenyl)corrole: potential insights into the insolubility of gold octabromocorroles, *J. Porphyrins Phthalocyanines* 22 (2018) 596–601.
- [30] K. Sudhakar, A. Mizrahi, M. Kosa, N. Fridman, B. Tumanskii, M. Saphier, Z. Gross, Effect of selective CF<sub>3</sub> substitution on the physical and chemical properties of gold corroles, *Angew. Chem. Int. Ed.* 56 (2017) 9837–9841.
- [31] M. Soll, K. Sudhakar, N. Fridman, A. Muller, B. Röder, Z. Gross, One-pot conversion of fluorophores to phosphophores, *Org. Lett.* 18 (2016) 5840–5843.
- [32] C.M. Lemon, D.C. Powers, P.J. Brothers, D.G. Nocera, Gold corroles as near-IR phosphors for oxygen sensing, *Inorg. Chem.* 56 (2017) 10991–10997.
- [33] W. Sinha, M.G. Sommer, M. van der Meer, S. Plebst, B. Sarkar, S. Kar, Structural, electrochemical and spectroelectrochemical study on the geometric and electronic structures of [(corrolato)Au<sup>III</sup>]<sub>n</sub> (n = 0, +1, -1) complexes, *Dalton Trans.* 45 (2016) 2914–2923.
- [34] J. Terner, V. Palaniappan, A. Gold, R. Weiss, M.M. Fitzgerald, A.M. Sullivan, C. M. Hosten, Resonance Raman spectroscopy of oxoiron(IV) porphyrin  $\pi$ -cation radical and oxoiron(IV) hemes in peroxidase intermediates, *J. Inorg. Biochem.* 1000 (2006) 480–501.
- [35] R. Weiss, D. Mandon, T. Wolter, A.X. Trautwein, M. Müther, E. Bill, A. Gold, K. Jayaraj, J. Terner, Delocalization over the heme and the axial ligands of one of the two oxidizing equivalents stored above the ferric state in the peroxidase and catalase compound-I intermediates: indirect participation of the proximal axial ligand of iron in the oxidation reactions catalyzed by heme-based peroxidases and catalases? *J. Biol. Inorg. Chem.* 1 (1996) 377–383.
- [36] A.J. Sitter, C.M. Reczek, J. Terner, Heme-linked ionization of horseradish peroxidase compound II monitored by the resonance Raman Fe(IV)=O stretching vibration, *J. Biol. Chem.* 260 (1985) 7515–7522.
- [37] J. Terner, A.J. Sitter, C.M. Reczek, Resonance Raman spectroscopic characterizations of horseradish peroxidase. Observations of the Fe<sup>IV</sup>=O stretching vibration of Compound II, *Biochim. Biophys. Acta* 828 (1989) 73–80.
- [38] C.M. Reczek, A.J. Sitter, J. Terner, Resonance Raman characterization of heme Fe (IV)=O groups of intermediates of yeast cytochrome C peroxidase and lactoperoxidase, *J. Mol. Struct.* 214 (1989) 27–41.
- [39] A.J. Sitter, C.M. Reczek, J. Terner, Observation of the Fe(IV)=O stretching vibration of ferryl myoglobin by resonance Raman spectroscopy, *Biochim. Biophys. Acta* 828 (1989) 229–235.
- [40] M.T. Green, J.H. Dawson, H. B., Gray Oxoiron(IV) in Chloroperoxidase compound II is basic: implications for P450 chemistry, *Science* 304 (2004) 1653–1656.
- [41] J. Terner, A. Gold, R. Weiss, D. Mandon, A.X. Trautwein, Symmetry states of metalloporphyrin  $\pi$ -cation radicals, models for peroxidase compound I, *J. Porphyrins Phthalocyanines* 5 (2001) 357–364.
- [42] A. Ghosh, Preface – 1950–2000: fifty years of theoretical research on porphyrins, *J. Porphyrins Phthalocyanines* 5 (2001) 187–189.
- [43] R. Weiss, V. Bulach, A. Gold, J. Terner, A.X. Trautwein, *J. Biol. Inorg. Chem.* 6 (2001) 831–845.
- [44] A. Ghosh, High-valent metalloporphyrins: metal- versus ligand-centered oxidation, *J. Biol. Inorg. Chem.* 6 (2001) 726.
- [45] A. Ghosh, High-valent iron intermediates in biology, *J. Inorg. Biochem.* 100 (2006) 419–420.
- [46] R. Weiss, A. Gold, J. Terner, Cytochromes c: biological models for the S = 3/2,5/2 spin-state admixture? *Chem. Rev.* 106 (2006) 2550–2579.
- [47] I.P.T. Filho, J. Terner, R.N. Pittman, L.G. Somera III, K.R. Ward, Hemoglobin oxygen saturation measurements using resonance Raman intravital microscopy, *Am. J. Physiol. Hear. Circ.* 289 (2005) H488–H495.
- [48] I.P.T. Filho, J. Terner, R.N. Pittman, E. Proffitt, K.R. Ward, Measurement of hemoglobin oxygen saturation using Raman microspectroscopy and 532-nm excitation, *J. Appl. Physiol.* 104 (2008) 1809–1817.
- [49] I.P.T. Filho, N.M. Nguyen, R. Jivani, J. Terner, P. Romfh, D. Vakshoori, K.R. Ward, Oxygen saturation monitoring using resonance Raman spectroscopy, *J. Surg. Res.* 201 (2016) 425–431.
- [50] A.B. Alemanyehu, K.J. Gagnon, J. Terner, A. Ghosh, Oxidative metalation as a route to size-mismatched macrocyclic complexes: osmium Corroles, *Angew. Chem. Int. Ed.* 53 (2014) 14411–14414.
- [51] J. Sankar, S. Mori, S. Saito, H. Rath, M. Suzuki, Y. Inokuma, H. Shinokubo, K. S. Kim, Z.S. Yoon, J.-Y. Shin, J.M. Lim, Y. Matsuzaki, O. Matsushita, A. Muranaka, N. Kobayashi, D. Kim, A. Osuka, Unambiguous identification of Möbius aromaticity for meso-aryl-substituted [28]hexaphyrins(1.1.1.1.1), *J. Am. Chem. Soc.* 130 (2008) 13568–13579.
- [52] Z. Gross, N. Galili, I. Saltsman, The first direct synthesis of corroles from pyrrole, *Angew. Chem. Int. Ed.* 38 (1999) 1427–1429.
- [53] Z. Gross, N. Galili, L. Simkovich, I. Saltsman, M. Botoshansky, D. Blaeser, R. Boese, I. Goldberg, Solvent-free condensation of pyrrole and pentafluorobenzaldehyde: a novel synthetic pathway to corrole and oligopyrromethenes, *Org. Lett.* 1 (1999) 599–602.
- [54] E. van Lenthe, E.J. Baerends, J.G. Snijders, Relativistic regular two-component Hamiltonians, *J. Chem. Phys.* 99 (1993) 4597–4610.
- [55] C. van Wüllen, Molecular density functional calculations in the regular relativistic approximation: method, application to coinage metal diatomics, hydrides, fluorides and chlorides, and comparison with first-order relativistic calculations, *J. Chem. Phys.* 109 (1998) 392–399.
- [56] J.P. Perdew, Density-functional approximation for the correlation energy of the inhomogeneous electron gas, *Phys. Rev. B* 33 (1986) 8822–8824.
- [57] A.D. Becke, Density-functional exchange-energy approximation with correct asymptotic behavior, *Phys. Rev. A* 38 (1988) 3098–3100.
- [58] A.D. Becke, Density-functional thermochemistry. III. The role of exact exchange, *J. Chem. Phys.* 98 (1993) 5648–5652.
- [59] C. Lee, W. Yang, R.G. Parr, Development of the Colle-Salvetti correlation-energy formula into a functional of the electron density, *Phys. Rev. B* 37 (1988) 785–789.
- [60] G. te Velde, F.M. Bickelhaupt, E.J. Baerends, C. Fonseca Guerra, S.J.A. van Gisbergen, J.G. Snijders, T. Ziegler, Chemistry with ADF, *J. Comput. Chem.* 22 (2001) 931–967.